International Journal of Thermal Sciences 200 (2024) 108935

Contents lists available at ScienceDirect

International Journal of Thermal Sciences

journal homepage: www.elsevier.com/locate/ijts

Dimensionless numerical sensitivity analysis of narrow cracks by means of infrared lock-in thermography

David Sagarduy-Marcos, Javier Rodríguez-Aseguinolaza *

Departamento de Física Aplicada, Escuela de Ingeniería de Bilbao, Universidad del País Vasco UPV/EHU, Plaza Ingeniero Torres Quevedo 1, Bilbao, 48013, Spain

ARTICLE INFO

Keywords:
Infrared thermography
Non-destructive narrow crack characterization
Numerical modeling
Dimensionless analysis
Sensitivity analysis

ABSTRACT

The non-destructive detection of defects in materials, such as cracks, delaminations and others, is a critical issue to be addressed in many technological applications like automotive, aeronautical or aerospace industries. In this frame, lock-in infrared thermography is identified as a highly suitable solution offering not only a qualitative detection of the defects but also their quantitative characterization. With the goal of maximizing its capabilities on the crack detection and characterization, in this work, a dimensionless numerical global sensitivity analysis of the lock-in infrared thermography is developed. First, a complete dimensionless reformulation of the thermographic investigation is provided, not only limited to the defect geometrical parameters, but also including the corresponding experimental parameters. As a consequence, the constraints of particular experimental setups or material properties can be removed by means of an appropriate choice of length, time and temperature scales. This leads to a set of dimensionless parameters and equations which preserve the full physical information of the experiment. The resulting model has been numerically solved and successfully validated by using experimental thermographic data over laboratory calibrated cracked material samples. Second, the developed dimensionless numerical model has been used as input for a global sensitivity analysis able to determine the correlations between the proposed dimensionless parameters and their corresponding impact on the thermographic results. Furthermore, the ranges of sensitivity and predominance of each dimensionless parameter are obtained, which provide quantitative parametric selection criteria for a maximized efficiency and accuracy on the thermographic crack detection and characterization.

1. Introduction

The detection and characterization of defects, such as cracks or delaminations, is a challenge and a necessity to prevent mechanical failures since they play an important role in the strength of a wide variety of structural and industrial components [1–3].

In order to detect and characterize potential defects, in addition to maintaining the integrity and further operability of the material, non-destructive testing (NDT) measurement techniques are identified as an appropriate alternative [4,5]. In this frame, infrared (IR) thermography has been proposed as a non-intrusive and safe method to detect quasi-superficial defects [6,7]. In particular, optical excitation has proven to be a high efficient alternative not only in the detection but also in the characterization of potential defects [8,9]. In this methodology, a light source provides energy to the sample producing an increase in surface temperature and hence, the diffusion of heat in the material. Consequently, any inner defect will be revealed by an abnormal temperature distribution in the images of the infrared radiation detected by a thermographic camera, called thermogram [10].

Multiple lighting alternatives can be found. On one hand, halogen or flash lamps can be chosen to illuminate the entire surface of the sample [11,12]. This would produce a heat flux in-depth and would allow the detection of defects parallel to the surface, such as corrosion or delaminations [13]. On the other hand, in-depth propagation and lateral heat flux, which might be disturbed by the presence of cracks, can be achieved by using a laser beam focused at the sample surface [14,15]. As a result, the thermogram would reveal a temperature discontinuity introduced by the presence of the crack [16].

Among all the lighting techniques, lock-in thermography is the one which allows an enhanced signal-to-noise ratio due to its benefits associated to signal filtering [17,18]. As a consequence, very small defects (in the order of microns) can successfully be measured, which has made this technique one of the most used in this field [8,19]. Even if the real deployment of this technique has to address with difficulties derived from the nature of complex materials, mixed thermophysical properties, large dimension samples, etc., they can be overcome under proper conditions. On one hand, a graphite layer can be sprayed to

* Corresponding author.
E-mail address: javier.rodriguezas@ehu.eus (J. Rodríguez-Aseguinolaza).

https://doi.org/10.1016/j.ijthermalsci.2024.108935
Received 29 March 2023; Received in revised form 30 May 2023; Accepted 25 January 2024
Available online 6 February 2024

homogenize the illuminated surface and enhance the IR emission [20,21]. On the other hand, in order to study the capabilities of infrared thermography applied to large samples, flying spot technique has also been proposed. This method enables the prospection by a continuous movement of the laser over the investigated sample [22,23].

However, even if experimental thermographic results provide a precise detection of potential material defects, laboratory measurements must be complemented with theoretical calculations in order to obtain a fully quantitative geometrical characterization of the involved defects [8]. When addressing the physical modeling of the thermographic problem, dimensional numerical models are conventionally developed [19,24]. Even if this strategy suits for particular setups or materials, the obtained results are not extensible to different experimental conditions.

Considering the aforementioned, the main objective of this work is double. First, to propose a general dimensionless view of the lock-in infrared thermography used for crack quantitative characterization, which provides an unconstrained understanding of the involved physical phenomena giving an insight into the fundamental scales of the problem. Second, using the developed dimensionless numerical model as input, to obtain a stochastic global sensitivity assessment able to determine the thermographic detection limits and optimal parametric set-ups for maximized crack detection capabilities in terms of sensitivity and cross parametric correlations.

2. Mathematical formulation

2.1. Dimensionless governing equations

The non-destructive inspection of potential cracks using laser-spot lock-in IR thermography consists of exciting the sample with a continuous laser beam of Gaussian profile whose intensity is modulated by means of a mechanical chopper [25]. Once the intensity is modulated, the laser is focused by an optical lens system and directed perpendicular to the sample surface using mirrors. In this configuration, the mirror must reflect the visible light and must also be transparent to the IR radiation in order to allow its recording by the thermographic camera [26]. Although the complete thermogram from the illuminated side of the sample is obtained, in this work the depicted results correspond to the central profile of the sample in the y direction. A diagram of the described experimental configuration can be seen in Fig. 1.

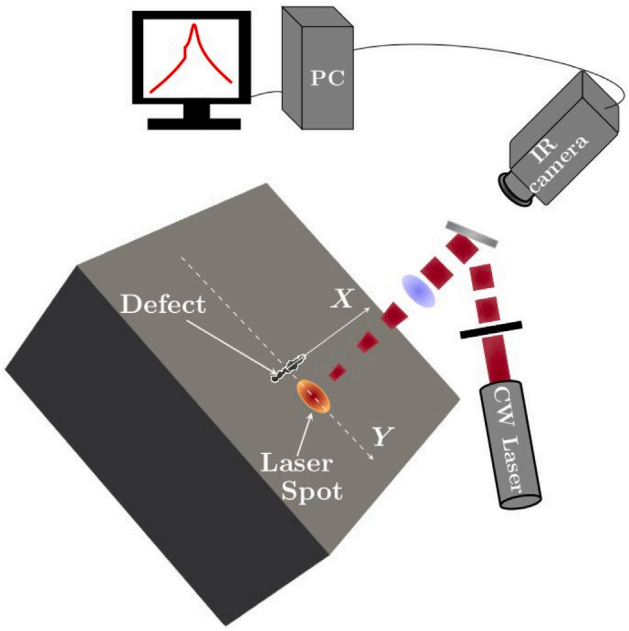

Fig. 1. Schematic view of a laser-spot lock-in IR experiment with a focused continuous wave (CW) laser beam used as optically illuminating source. The dashed line indicates the profile where the temperatures are obtained.

Considering the diffusive nature of the studied problem, the constitutive dimensional equation is the heat equation Eq. (1).

$$\nabla^2 T = \frac{1}{\alpha}\frac{\partial T}{\partial t} \tag{1}$$

where α is the thermal diffusivity.

Due to the harmonic nature of the heating source, after the stationary state is attained, the temperature oscillates harmonically and the constant continuous heating contribution over room temperature can be removed. Therefore, the boundary condition associated with the illumination can be written as Eq. (2).

$$-\kappa \nabla T|_{\text{illuminated}} = A(x,y)\eta \cos(2\pi f t) \tag{2}$$

being f the modulation frequency, κ the thermal conductivity of the material, η the power fraction absorbed by the sample and $A(x,y)$ a parameter that depends on the spatial shape of the illumination. If the heating source is a CW laser of power P centered at $(0, y_0, 0)$, focused to a radius r_g and whose profile is assumed to be Gaussian, then $A(x,y)$ is given by Eq. (3).

$$A(x,y) = \frac{2P}{\pi r_g^2} e^{-2\left[\left(\frac{x}{r_g}\right)^2 + \left(\frac{y-y_0}{r_g}\right)^2\right]} \tag{3}$$

It has to be mentioned that, in the following, the negative sign of Eq. (2) is removed and introduced as a phase in the modulation term. For the remaining boundaries adiabatic thermal condition is assumed [27] as stated in Eq. (4).

$$-\kappa \nabla T|_{\text{non-illuminated}} = 0 \tag{4}$$

The continuity of the heat flow through the crack and the involved temperature jump are introduced by Eqs. (5) and (6) respectively.

$$[[-\kappa \nabla T]]|_{\text{crack}} = 0 \tag{5}$$

$$\Delta T|_{\text{crack}} = \kappa R_{th} \nabla T \tag{6}$$

where [[ ]] stands for the jump operator. In this work, the crack is modeled as a thermal contact resistance R_{th} [10], related to the width (w) of the crack through Eq. (7).

$$R_{th} = \frac{w}{\kappa_d} \tag{7}$$

being κ_d the thermal conductivity of the material filling the crack, usually assumed to be air. It is worth to notice that Eq. (7) implies that the width of the defect is, on one hand, narrow enough to neglect convective heat transfer [28] and, on the other hand, wide enough to prevent ballistic heat transfer [29]. In practice, in the developed model, micron-scale fissures are addressed. It can be noted that the established Eqs. (1)–(7), are not only limited to cracks, but can also be extended for other type of defects, such as delaminations, in the mentioned validity range. Moreover, although the thermal resistance of the defect is supposed to be constant in this work, it could also be modeled with a spatial dependency.

In order to obtain a dimensionless formulation, characteristic length L_c, time t_c and temperature T_c scales must be introduced. First, thermal diffusion length (μ) is selected as a natural length scale as shown in Eq. (8). This selection is made since μ is the distance from the modulated heat source where an appreciable energy transfer takes place [30].

$$L_c \equiv \mu \equiv \sqrt{\frac{\alpha}{\pi f}} \tag{8}$$

Second, considering the harmonic nature of the illumination, the inverse of the modulation frequency has been selected as characteristic

time scale Eq. (9).

$$t_c \equiv \frac{1}{2\pi f} \tag{9}$$

Finally, the characteristic temperature scale can be selected as the one removing the dimensions from Fourier equation, shown in Eq. (10).

$$T_c \equiv \frac{P\eta}{\mu\kappa} \tag{10}$$

Overall, for convenience, the time and temperature scales are multiplied by a factor 2 and $1/\pi$ respectively. Introducing these scales in Eqs. (1), (3), (5) and (6), the dimensionless set of equations that describe the laser-spot lock-in thermography experiment are obtained (11).

$$\begin{cases} \bar{\nabla}^2\bar{T} = \frac{\partial\bar{T}}{\partial\bar{t}} \\ \bar{\nabla}\bar{T}|_{\text{illuminated}} = 2\left(\frac{\mu}{r_g}\right)^2 e^{-2\left[\left(\frac{\bar{x}}{r_g/\mu}\right)^2+\left(\frac{\bar{y}-\bar{y}_0}{r_g/\mu}\right)^2\right]}\cos(2\bar{t}) \\ \bar{\nabla}\bar{T}|_{\text{non-illuminated}} = 0 \\ [[\bar{\nabla}\bar{T}]]|_{\text{crack}} = 0 \\ \Delta\bar{T}|_{\text{crack}} = \frac{\kappa R_{th}}{\mu}\bar{\nabla}\bar{T} \end{cases} \tag{11}$$

Here the barred variables refer to dimensionless quantities. Rearranging the parameters and defining $\Pi_1 \equiv 2(\mu/r_g)^2$ and $\Pi_2 \equiv \kappa R_{th}/\mu$, the set of Eqs. (11) can be rewritten as Eqs. (12).

$$\begin{cases} \bar{\nabla}^2\bar{T} = \frac{\partial\bar{T}}{\partial\bar{t}} \\ \bar{\nabla}\bar{T}|_{\text{illuminated}} = \Pi_1 e^{-\Pi_1\left[\bar{x}^2+(\bar{y}-\Pi_6)^2\right]}\cos(2\bar{t}) \\ \bar{\nabla}\bar{T}|_{\text{non-illuminated}} = 0 \\ [[\bar{\nabla}\bar{T}]]|_{\text{crack}} = 0 \\ \Delta\bar{T}|_{\text{crack}} = \Pi_2\bar{\nabla}\bar{T} \end{cases} \tag{12}$$

As can be seen in the set of Eqs. (12) this model does not imply any geometrical restriction for the crack. However, for practical purposes, this work has been carried out considering planar open-surface cracks as shown in Fig. 2. As a consequence, the crack is fully characterized by two spatial parameters, length (l) and depth (d), and the inclination angle (θ) measured from the illuminated side ($\bar{y} > 0$) of the sample. According to the selected characteristic length scale the two spatial parameters must be rescaled as $\Pi_3 \equiv l/\mu$ and $\Pi_4 \equiv d/\mu$. In order to maintain the same notation for all the dimensionless parameters, $\Pi_5 \equiv \theta$ and $\Pi_6 \equiv \bar{y}_0$.

The set of Eqs. (12) has been numerically solved by using Open Source Field Operation and Manipulation (OpenFoam) [31] software in a workstation with an Intel Xeon(R) Gold 5218 CPU @ 2.30 GHz × 64, 192 Gb memory.

2.2. Computational domain

The inclusion of narrow micron-scale defects in large spatial domains represents a big challenge due to the different length scales between them. A big effort has been done in order to numerically investigate narrow defects meshing their full volume and also considering the convective and radiative heat transfer phenomena inside them [32,33]. Even if the obtained results successfully describe the considered physical problem, this meshing strategy can lead to very fine meshes increasing memory resources and calculation time. Alternatively, in order to take advantage of coarser meshes and the related computational economy, the planar crack has been introduced as a 2D interface in the domain [10,19], as shown in Fig. 2. This interface is characterized by a thermal resistance given by Eq. (7) and introduced in the dimensionless formulation in the Π_2 parameter.

Taking into account the need of capturing diverse crack inclination angles and geometries, a flexible meshing must be considered. In these terms, a tetrahedral topology mesh with dimensions $10 \times 10 \times 5$ is used.

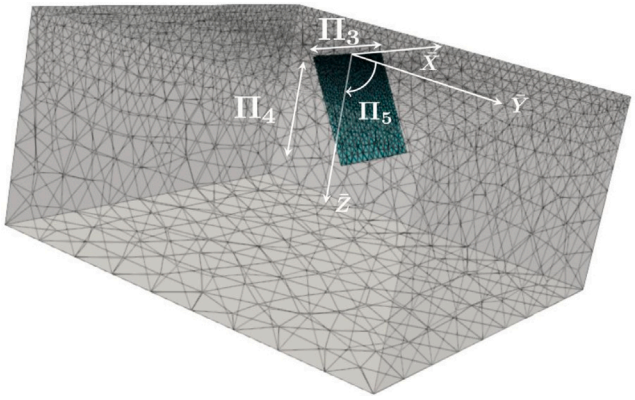

Fig. 2. Spatial discretization used in the developed numerical model. The highlighted 2D interface corresponds to the modeled planar open-surface crack.

Table 1
Obtained RMSE and NRMSE between the selected experimental and numerical benchmark cases.

Case	RMSE (a.u.)	NRMSE (%)
$w = 5$ μm, $\theta = 60°$	0.17	3.6
$w = 10$ μm, $\theta = 120°$	0.22	4.9

Note that these dimensions ensure no border effects as the thermal diffusion length (μ) is considered as characteristic length scale. With the objective of accurately reproduce all the involved thermal effects, a spatially variable mesh resolution is implemented. The laser spot and the sampling profile regions (see Fig. 1) present a mesh resolution around 0.1% of the sample length in the plane perpendicular to the illumination. On the other hand, the regions far from the physical interest zones, such as the opposite face of the illumination, have a decreased resolution up to around 10%. As a result, $\approx 10^4$ (average) mesh elements are used in this work with an associated calculation time of around 2 min for a fully parallelized computation with 8 processors.

3. Model validation

In order to demonstrate the accuracy of the developed model, experimental data from Ref. [10], corresponding to the natural logarithm of the obtained normalized amplitude of the temperature oscillation ($\ln|\tau_n|$) over the central profile of the sample in the y direction, according to Fig. 1, has been used. As explained in [10], the crack is experimentally introduced by means of calibrated separating tapes between two pieces of a reference material, in this case AISI-304 stainless steel, presenting an inclined contact interface with a controlled angle. In practice, the resulting laboratory crack model consists on a infinite depth and length ($d, l \gg \mu$) crack with fixed width and angle. For benchmark comparison, two experimental cases have been considered, one for $w = 5$ μm and $\theta = 60°$ and the second for $w = 10$ μm and $\theta = 120°$. The experimental temperature data is obtained using an IR video camera (256 × 320 px) where a 30 μm square of the sample is sensed. For the rest of experimental/material parameter details, see [10].

As can be seen in Fig. 3, in all benchmark cases the developed numerical model and experimental results show a very good agreement. The quantification of the obtained error between the experimental and numerical results is computed by means of the root mean squared error (RMSE) and normalized RMSE (NRMSE), showing very reduced values as summarized in Table 1. It has to be noted the NRMSE has been computed dividing the absolute RMSE by the norm of the signal. The small discrepancies revealed by these results can be ascribed with two main aspects. First, the experimental point spread function (PSF) associated to the discontinuity introduced by the crack does not exactly fit the model, which assumes the crack as a 2D interface. Second, the

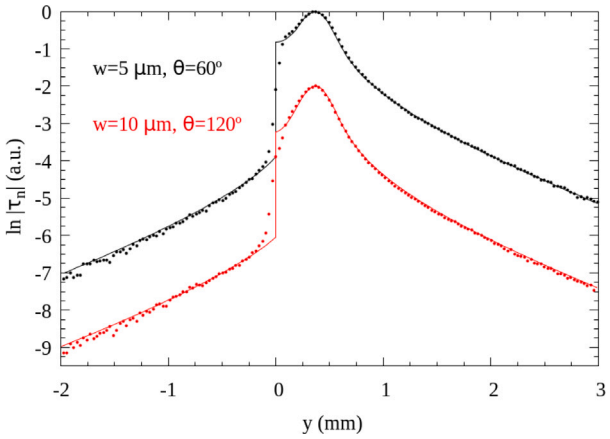

Fig. 3. Comparison between the experimental (dots) [10] and dimensionless numerical model (continuous line). Experiments were performed for AISI-304 with the following experimental parameters: $P = 0.1$ W, $f = 0.8$ Hz, $r_g = 0.2$ mm and $y_0 = 0.4$ mm. For the sake of clarity, the profiles have been shifted vertically.

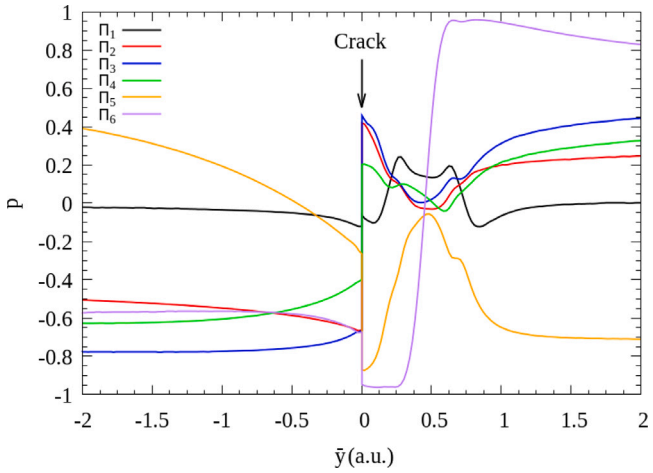

Fig. 4. Obtained partial correlation coefficient (p) distributions for each dimensionless parameter as a function of the spatial coordinate.

Table 2
Dimensionless parameters and their corresponding ranges considered in the LHS global sensitivity analysis.

Dimensionless parameter	Considered range
$\Pi_1 = 2(\mu/r_g)^2$	[15,500]
$\Pi_2 = \kappa w/(\kappa_{air}\mu)$	[0.0001,10]
$\Pi_3 = l/\mu$	[0.1,3]
$\Pi_4 = d/\mu$	[0.1,2]
$\Pi_5 = \theta$ (°)	[30,150]
$\Pi_6 = y_0/\mu$	[0.2,0.7]

uncertainties related to the experimental setup parameters together with the inherent measurement increasing noise at low signal values also lead to small discrepancies. Finally, it is worth to mention that further phenomena, such as the black-body effect [34], are not included in this model since a very narrow crack with an ideal planar geometry is assumed. However, the obtained error in all the studied benchmark cases is below 5%, which guarantees the validity of the model.

4. Global sensitivity analysis and discussion

Once the dimensionless numerical model has been constructed and validated, it has been used as input to a global sensitivity analysis. As a result, the correlations between the proposed dimensionless parameters and their impact on the thermographic results are determined. For an appropriate statistical approach, the probe space has been stochastically sampled on 1000 test cases by using the Latin Hypercube Sampling (LHS) algorithm [35]. Table 2 shows the studied parametric ranges which configure the LHS probe space. It is worth mentioning that these intervals have been selected balancing, on one hand, the consideration of cases with practical interest and, on the other hand, the accuracy of the sensitivity analysis results on interest parametric ranges.

4.1. Dimensionless parameter correlation analysis

The sensitivity to each dimensionless parameter is quantified by the partial correlation coefficient (p) [36] which measures the correlation between the natural logarithm of the amplitude of the dimensionless temperature oscillation ($\ln|\bar{\tau}|$), and the dimensionless parameter while accounting for the effects of the others'. A perfect linear relationship between variables and the $\ln|\bar{\tau}|$ is obtained when $|p| = 1$, while the sign shows if their dependency is direct (+) or inverse (−). On the other hand, the value $p = 0$ means that there is not correlation between them. As mentioned in previous sections, the computed results, shown in Fig. 4, are obtained as a function of the spatial coordinate for the central profile of the sample in the $\bar{y}$ direction according to Fig. 1.

From Fig. 4, as a common trend, all the parameters show a sensitivity decrease in the Π_6 variation range, which can be dimensionally explained in terms of the involved excitation energy, which strongly limits the potential signal contrast for any further effect detection.

Π_1 shows a very poor sensitivity in the complete spatial range with an slight increase close to the laser-spot. Π_2 shows a slightly increasing sensitivity when approaching the crack from $\bar{y} < 0$ region, whereas the obtained value is nearly constant, but not negligible, far from the crack at $\bar{y} > 0$. Π_3 and Π_4 show a noticeable sensitivity in the complete spatial range, which is reinforced in the $\bar{y} < 0$ region with a decreasing sensitivity trend when approaching the crack. In addition, for both parameters, the computed results reveal a proportional sensitivity trend in the complete range, which means that they are highly correlated. Π_5 shows a larger and nearly constant sensitivity at $\bar{y} > 0$ far from the crack whereas a strong decreasing sensitivity trend is found in the $\bar{y} < 0$ region. Π_6 shows a drastic sensitivity change from an inverse to direct proportionality between the limits of the associated range at $\bar{y} > 0$ region. In addition, a slight sensitivity increase is observed close to the crack at $\bar{y} < 0$, similar to the one associated to Π_2.

It must be highlighted that Fig. 4 shows no coupling between the proposed dimensionless parameters exception made for Π_3 and Π_4. However, even if small, slight uncoupling can be observed close to the crack position in the $\bar{y} < 0$ region. In any case, the potential uncoupling of both mentioned parameters can be strongly dependent on the quality of the thermographic experimental results, leading to possible difficulties associated to experimental noise, uncertainties or other inaccuracies.

4.2. Model response analysis

In order to complement the spatial sensitivity information given by the partial correlation coefficient in Fig. 4, considering the obtained distributions, the model response as a function of each parameter value is shown in the maximum sensitivity regions in Fig. 5. In these plots two key aspects can be assessed through the obtained trend and response dispersion. The trend highlighted with a red line on Fig. 5 is used as a visual guide. In this case, the parametric sensitivity range is presented on non-zero slope regions. In addition, the increasing or decreasing behavior of the model response as a function of each dimensionless parameter value is also obtained. Regarding the dispersion, its decrease can be associated to an increasing influence of the parameter on the

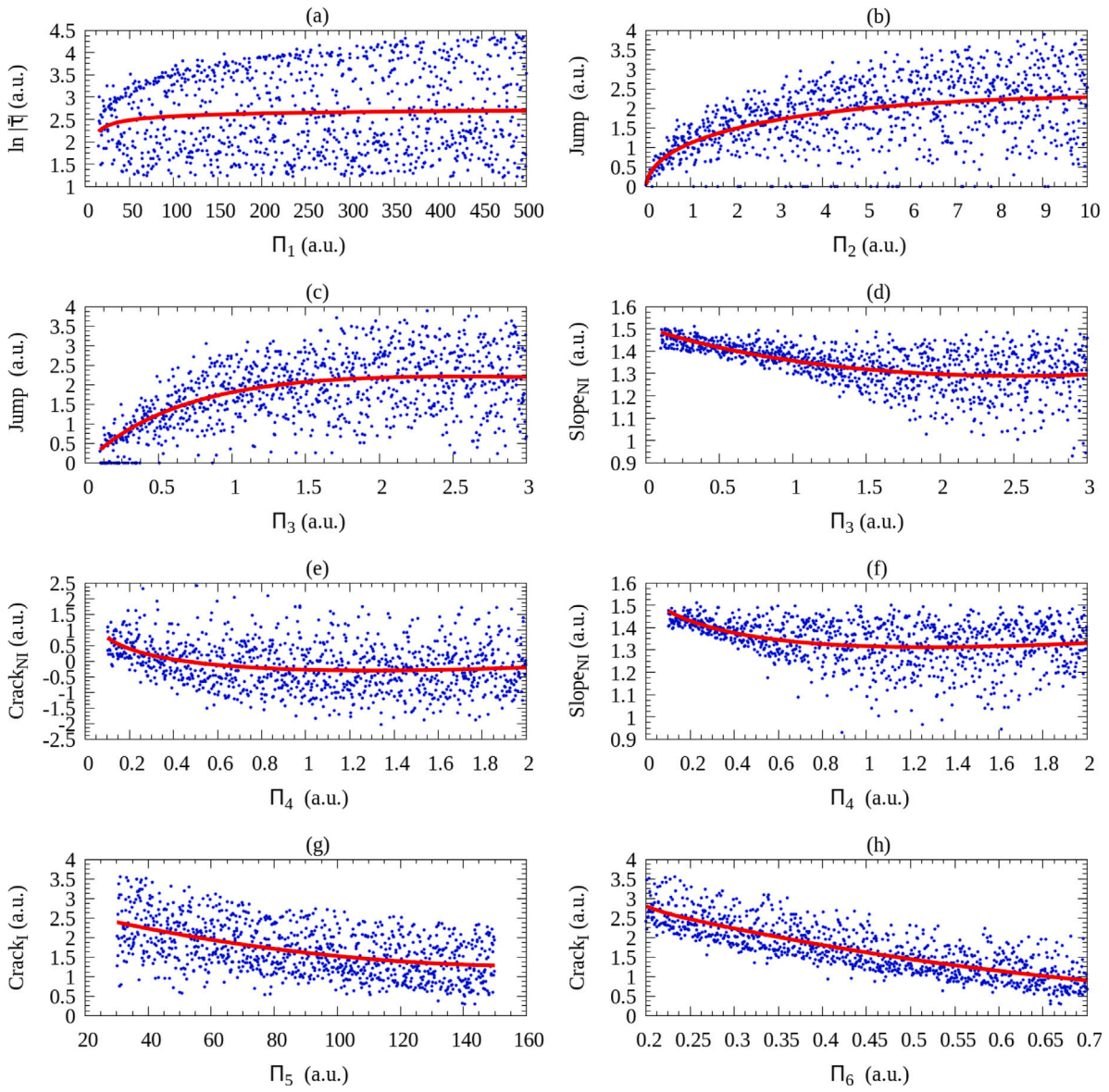

Fig. 5. Scatter plots of the selected model responses as a function of (a) Π_1, (b) Π_2, (c) and (d) Π_3, (e) and (f) Π_4, (g) Π_5 and (h) Π_6. The red line represents a visual scatter trend guide.

obtained model response and vice versa. In these terms, null dispersion must be understood as an univocal relation between the model response and the selected parameter, hereafter discussed as predominancy. In the following, a quantitative sensitivity discussion is given for each dimensionless parameter.

4.2.1. Π_1

Considering the partial correlation coefficient results for Π_1, shown in Fig. 4, even if slightly larger values are obtained close to the laser-spot, no clearly preferential sensitivity space regions are identified. As a consequence, $\ln|\bar{\tau}|$ is selected as model response, depicted in Fig. 5(a). The obtained trend is nearly flat, which indicates a very poor sensitivity for this parameter in the complete studied range. However, slightly increasing sensitivity is obtained for Π_1 decreasing values, in the $\Pi_1 \lesssim 100$ range. In addition, in the same parametric range, a small decrease of the dispersion is also observed.

4.2.2. Π_2

The effect of this parameter can be observed in the complete studied spatial range as shown in Fig. 4. Nevertheless, its influence is more remarkable in the discontinuity introduced by the crack at $\bar{y} = 0$, hereafter denoted as "jump" and calculated as the difference between the model responses in the illuminated ("Crack_I") and non-illuminated ("Crack_NI") limits of the crack.

As can be observed in Fig. 5(b), the decreasing trend and dispersion obtained for the selected response indicates that both, the sensitivity and predominance are increased for $\Pi_2 \lesssim 5$. Moreover, it must be noted that for values $\Pi_2 \lesssim 1$ the jump response is, in essence, determined by this parameter.

4.2.3. Π_3

As can be seen in Fig. 4, the influence in the spatial model response of this parameter is double. First, a clear impact on the discontinuity introduced by the crack can be observed Fig. 5(c). Second, the model response at the non-illuminated side of the sample also presents a noticeable influence, far from the crack. In this range a quasi-linear behavior of $\ln|\bar{\tau}|$ is obtained, as can be seen in Fig. 3. As a consequence, taking into account both phenomena, the jump and the slope on the non-illuminated side ("Slope_NI") are used as significant model responses, shown in Fig. 5(c) and (d) respectively. In both cases, the

Table 3
Upper limits of sensitivity and predominance ranges concluded from the global sensitivity analysis results.

Dimensionless parameter	Upper limit	
	Sensitivity	Predominance
Π_1	100	100
Π_2	5	1
Π_3	1.5	0.5
Π_4	1	0.5
Π_5	140	–
Π_6	Full range	–

sensitivity and predominance are increased for decreasing values of Π_3 with opposite response trends.

However, it must be noted that even if the sensitivity range for the Slope_{NI} is slightly extended, its magnitude is significantly lower than the one obtained for the jump response. Overall, considering both model responses, it can be concluded that the optimal sensitivity range is $\Pi_3 \lesssim 1.5$.

4.2.4. Π_4

As mentioned in Section 4.1, Π_4 and Π_3 show a clear correlation in the complete studied spatial range. As a consequence, similar spatial influence regions can be expected together with increasing sensitivity for decreasing parameter values. However, as can be seen in Fig. 4, the sensitivity obtained for Crack_{I} is almost negligible and, therefore, the selection of the jump as a model response is not convenient. Instead, the Crack_{NI} response provides a more appropriate view of the sensitivity.

According to Fig. 5(e) and (f), the obtained increasing trends for decreasing parameter values reveal that the sensitivity range for this parameter is for $\Pi_4 < 1$. It is noteworthy that, even if Π_3 and Π_4 are highly correlated, their corresponding parametric sensitivity and predominance ranges are noticeably different being the ones of Π_4 clearly reduced.

4.2.5. Π_5

According to Fig. 4, the maximum sensitivity for this parameter is obtained for the illuminated side of the sample close to the crack (Crack_{I}), used as model response in Fig. 5(g). As can be seen, an increasing sensitivity for decreasing Π_5 values is obtained. Considering that the inclination angle is measured from the illuminated side of the sample ($\bar{y} > 0$), this behavior can be explained since lower angles mean less distance between the heat source and the crack. Accordingly, large values of Π_5 subtend crack positions beyond the thermal diffusion length leading to a sensitivity decrease. However, even in this case, its impact in the selected model response is found to be not negligible, resulting into a sensitivity range of $\Pi_5 \lesssim 140°$. Regarding its predominance on the model response, no preferential parametric ranges are observed.

4.2.6. Π_6

Even if the partial correlation coefficient computed for Π_6 shown in Fig. 4 reveals a very large value in the illuminated side of the sample, Crack_{I} is selected as significant model response for its sensitivity analysis, as depicted in Fig. 5(h). In this case, no preferential sensitivity neither predominance is observed.

Overall Table 3 summarizes the upper limits for optimal sensitivity and predominance ranges for all the proposed dimensionless parameters. Note that these results have been obtained for idealized results without having considered any added noise representing random or systematic errors, which depend on particular experimental set-ups. This approach is also supported by the fact that very high signal to noise ratios can be attained in lock-in thermography experiments. In addition, this model does not consider heat losses as they are negligible in a wide range of experimental parametric conditions [37]. As a consequence, the provided sensitivity ranges can be used as a realistic guideline in order to find the optimal experimental conditions for particular set-ups, materials and crack sizes. Moreover, in order to complement the sensitivity information, the predominance ranges are also included in Table 3. Considering the given interpretation of predominance as the prevalence of the parameter on the model response, these ranges favor the accuracy on the determination of each dimensionless parameter from termographic data by means of direct measurements or inverse optimization methods.

5. Conclusions

A dimensionless model of the lock-in infrared thermography used for the detection of micron-scale cracks is developed in this work. As a result, all the involved physical information is reduced to the six proposed dimensionless parameters including the experimental set-up configuration together with geometrical issues of the studied open surface cracks. The resulting equations are numerically solved and used as input in a global sensitivity analysis. Two main results are obtained from these calculations.

First the direct or inverse relation of the response with each dimensionless parameter has been determined together with the associated sensitivity. In this frame, it is concluded that all the proposed dimensionless parameters show an uncoupled behavior exception made of Π_3 and Π_4, which are found to be highly correlated in the full spatial range.

Second, the maximum spatial sensitivity regions together with the predominance of each dimensionless parameter have been identified. Leading apart the thermographic experimental parameters and material properties, the sensitivity obtained for Π_2, Π_3 and Π_4 reveals that laser-spot lock-in infrared thermography is an outstanding experimental technique when dealing with a quantitative analysis of narrow or small cracks, since the computed sensitivities show a clear increase for decreasing crack length, depth and width values. Moreover, the provided quantitative dimensionless parametric sensitivity ranges can be used as experiment guideline for optimal lock-in thermographic investigation of narrow open-surface cracks in materials.

CRediT authorship contribution statement

David Sagarduy-Marcos: Conceptualization, Methodology, Writing – original draft, Review, Software. **Javier Rodríguez-Aseguinolaza:** Conceptualization, Methodology, Writing – original draft, Review, Software.

Declaration of competing interest

The authors declare that they have no known competing financial interests or personal relationships that could have appeared to influence the work reported in this paper.

Data availability

Data will be made available on request.

Acknowledgments

This work has been supported by Ministerio de Ciencia e Innovación, Spain (Grant PID2019-104347RB-I00 funded by MCIN/AEI/10.13039/501100011033) and by Departamento de Educación del Gobierno Vasco (IT1430-22). This work was carried out within the framework of the Joint Cross-Border Laboratory (LTC) AENIGME (Aquitaine Euskadi Network In Green Manufacturing and Ecodesign). The authors would like to thank the Basque Government and EUSKAMPUS (LTC Sarea initiative) for their financial support for this LTC and this research work.

References

[1] R.A. Osornio-Rios, J.A. Antonino-Daviu, R. de Jesus Romero-Troncoso, Recent industrial applications of infrared thermography: A review, IEEE Trans. Ind. Inform. 15 (2) (2018) 615–625.

[2] Y. Cao, W. Zhu, J. Yang, G. Fu, D. Lin, Y. Cao, An effective industrial defect classification method under the few-shot setting via two-stream training, Opt. Lasers Eng. 161 (2023) 107294.

[3] S. Bagavathiappan, B.B. Lahiri, T. Saravanan, J. Philip, T. Jayakumar, Infrared thermography for condition monitoring–A review, Infrared Phys. Technol. 60 (2013) 35–55.

[4] L. Cartz, Nondestructive testing. URL https://www.osti.gov/biblio/260617.

[5] A. Chrysafi, N. Athanasopoulos, N. Siakavellas, Damage detection on composite materials with active thermography and digital image processing, Int. J. Therm. Sci. 116 (2017) 242–253.

[6] E.J. Kubiak, Infrared detection of fatigue cracks and other near-surface defects, Appl. Opt. 7 (9) (1968) 1743–1747.

[7] C. Meola, G.M. Carlomagno, A. Squillace, G. Giorleo, Non-destructive control of industrial materials by means of lock-in thermography, Meas. Sci. Technol. 13 (10) (2002) 1583.

[8] N. Pech-May, A. Oleaga, A. Mendioroz, A. Omella, R. Celorrio, A. Salazar, Vertical cracks characterization using lock-in thermography: I infinite cracks, Meas. Sci. Technol. 25 (11) (2014) 115601.

[9] R. Yang, Y. He, Optically and non-optically excited thermography for composites: A review, Infrared Phys. Technol. 75 (2016) 26–50.

[10] J. Rodríguez-Aseguinolaza, M. Colom, J. González, A. Mendioroz, A. Salazar, Quantifying the width and angle of inclined cracks using laser-spot lock-in thermography, NDT E Int. 122 (2021) 102494.

[11] A.R. Silva, M. Vaz, S. Leite, J. Gabriel, Lock-in thermal test with corrected optical stimulation, Quant. InfraRed Thermogr. J. 19 (4) (2022) 261–282, http://dx.doi.org/10.1080/17686733.2021.1933698, arXiv:https://doi.org/10.1080/17686733.2021.1933698.

[12] D. Hoffmann, M. Bastian, G. Schober, New approach for layer thickness measurements of coatings using pulsed lock-in thermography, Quant. InfraRed Thermogr. J. 19 (2) (2022) 71–84, http://dx.doi.org/10.1080/17686733.2020.1816752, arXiv:https://doi.org/10.1080/17686733.2020.1816752.

[13] T. Li, D.P. Almond, D.A.S. Rees, Crack imaging by scanning laser-line thermography and laser-spot thermography, Meas. Sci. Technol. 22 (3) (2011) 035701.

[14] J. González, A. Bedoya, A. Mendioroz, A. Salazar, Measuring the thermal resistance of vertical interfaces separating two different media using infrared thermography, Int. J. Therm. Sci. 135 (2019) 410–416.

[15] T. Archer, P. Beauchêne, B. Passilly, J.-M. Roche, Use of laser spot thermography for the non-destructive imaging of thermal fatigue microcracking of a coated ceramic matrix composite, Quant. InfraRed Thermogr. J. 18 (3) (2021) 141–158, http://dx.doi.org/10.1080/17686733.2019.1705732, arXiv:https://doi.org/10.1080/17686733.2019.1705732.

[16] M. Streza, Y. Fedala, J. Roger, G. Tessier, C. Boue, Heat transfer modeling for surface crack depth evaluation, Meas. Sci. Technol. 24 (4) (2013) 045602.

[17] A. Salazar, M. Colom, A. Mendioroz, Laser-spot step-heating thermography to measure the thermal diffusivity of solids, Int. J. Therm. Sci. 170 (2021) 107124.

[18] O. Breitenstein, W. Warta, M. Langenkamp, Lock-in Thermography: Basics and Use for Evaluating Electronic Devices and Materials, vol. 10, Springer, 2010.

[19] R. Celorrio, A. Omella, N. Pech-May, A. Oleaga, A. Mendioroz, A. Salazar, Vertical cracks characterization using lock-in thermography: II finite cracks, Meas. Sci. Technol. 25 (11) (2014) 115602.

[20] A. Salazar, A. Mendioroz, A. Oleaga, Flying spot thermography: Quantitative assessment of thermal diffusivity and crack width, J. Appl. Phys. 127 (13) (2020) 131101.

[21] M. Colom Serra, J. Rodríguez Aseguinolaza, M.A. Mendioroz Astigarraga, A. Salazar Hernández, Sizing the depth and width of narrow cracks in real parts by laser-spot lock-in thermography, 2021.

[22] E.J. Kubiak, Infrared detection of fatigue cracks and other near-surface defects, Appl. Opt. 7 (9) (1968) 1743–1747.

[23] Y. Wang, P. Kuo, L. Favro, R. Thomas, A novel "flying-spot" infrared camera for imaging very fast thermal-wave phenomena, in: Photoacoustic and Photothermal Phenomena II: Proceedings of the 6th International Topical Meeting, Baltimore, Maryland, July 31–August 3, 1989, Springer, 1990, pp. 24–26.

[24] J. Schlichting, C. Maierhofer, M. Kreutzbruck, Crack sizing by laser excited thermography, NDT & E Int. 45 (1) (2012) 133–140.

[25] Á. Cifuentes, A. Mendioroz, A. Salazar, Simultaneous measurements of the thermal diffusivity and conductivity of thermal insulators using lock-in infrared thermography, Int. J. Therm. Sci. 121 (2017) 305–312.

[26] M. Colom, J. Rodriguez-Aseguinolaza, A. Mendioroz, A. Salazar, Imaging real cracks: evaluation of the depth and width of narrow fatigue cracks in and al-alloys using laser-spot lock-in thermography, in: Thermosense: Thermal Infrared Applications XLIII, Vol. 11743, International Society for Optics and Photonics, 2021, 117430F.

[27] J. González, A. Mendioroz, A. Sommier, J. Batsale, C. Pradere, A. Salazar, Fast sizing of the width of infinite vertical cracks using constant velocity flying-spot thermography, NDT & E Int. 103 (2019) 166–172.

[28] L.C. Burmeister, Convective Heat Transfer, John Wiley & Sons, 1993.

[29] G. Chen, Ballistic-diffusive equations for transient heat conduction from nano to macroscales, J. Heat Transf. 124 (2) (2002) 320–328.

[30] E. Marín, Characteristic dimensions for heat transfer, Lat.-Am. J. Phys. Educ. 4 (1) (2010) 56–60.

[31] H.G. Weller, G. Tabor, H. Jasak, C. Fureby, A tensorial approach to computational continuum mechanics using object-oriented techniques, Comput. Phys. 12 (6) (1998) 620–631.

[32] N.J. Wallace, N.B. Crane, M.R. Jones, Defect measurement limits using flash thermography with application to additive manufacturing, NDT & E Int. 128 (2022) 102615.

[33] M. Krishnapillai, R. Jones, I.H. Marshall, M. Bannister, N. Rajic, NDTE using pulse thermography: Numerical modeling of composite subsurface defects, Compos. Struct. 75 (1–4) (2006) 241–249.

[34] Y. Wang, A. Charbal, F. Hild, S. Roux, L. Vincent, Crack initiation and propagation under thermal fatigue of austenitic stainless steel, Int. J. Fatigue 124 (2019) 149–166.

[35] M.D. McKay, R.J. Beckman, W.J. Conover, A comparison of three methods for selecting values of input variables in the analysis of output from a computer code, Technometrics 42 (1) (2000) 55–61.

[36] K. Baba, R. Shibata, M. Sibuya, Partial correlation and conditional correlation as measures of conditional independence, Aust. N. Z. J. Stat. 46 (4) (2004) 657–664.

[37] A. Salazar, A. Mendioroz, R. Fuente, The strong influence of heat losses on the accurate measurement of thermal diffusivity using lock-in thermography, Appl. Phys. Lett. 95 (12) (2009) 121905.